3D-Printed Reinforcement Scaffolds with Targeted Biodegradation Properties for the Tissue Engineering of Articular Cartilage

Journal Article

Author(s):
Tosoratti, Enrico; Fisch, Philipp; Taylor, Scott; Laurent-Applegate, Lee Ann; Zenobi-Wong, Marcy

Publication date:
2021-12-08

Permanent link:
https://doi.org/10.3929/ethz-b-000511951

Originally published in:
Advanced Healthcare Materials 10(23), https://doi.org/10.1002/adhm.202101094

ADVANCED HEALTHCARE MATERIALS
www.advhealthmat.de

3D-Printed Reinforcement Scaffolds with Targeted Biodegradation Properties for the Tissue Engineering of Articular Cartilage

*Enrico Tosoratti, Philipp Fisch, Scott Taylor, Lee Ann Laurent-Applegate, and Marcy Zenobi-Wong**

Achieving regeneration of articular cartilage is challenging due to the low healing capacity of the tissue. Appropriate selection of cell source, hydrogel, and scaffold materials are critical to obtain good integration and long-term stability of implants in native tissues. Specifically, biomechanical stability and in vivo integration can be improved if the rate of degradation of the scaffold material matches the stiffening of the sample by extracellular matrix secretion of the encapsulated cells. To this end, a novel 3D-printed lactide copolymer is presented as a reinforcement scaffold for an enzymatically crosslinked hyaluronic acid hydrogel. In this system, the biodegradable properties of the reinforced scaffold are matched to the matrix deposition of articular chondrocytes embedded in the hydrogel. The lactide reinforcement provides stability to the soft hydrogel in the early stages, allowing the composite to be directly implanted in vivo with no need for a preculture period. Compared to pure cellular hydrogels, maturation and matrix secretion remain unaffected by the reinforced scaffold. Furthermore, excellent biocompatibility and production of glycosaminoglycans and collagens are observed at all timepoints. Finally, in vivo subcutaneous implantation in nude mice shows cartilage-like tissue maturation, indicating the possibility for the use of these composite materials in one-step surgical procedures.

1. Introduction

Articular cartilage is a connective tissue lining diarthrodial joints of the human skeleton. Its primary function is to allow movement of the joint in a friction-free manner.[1] In 2010, the World Health Organization reported that 49.7% of the population above 65 years of age showed signs of cartilage degeneration, a number that is predicted to rise with a worldwide aging population. By 2030, cartilage degeneration is expected to be one of the highest causes of disability in the general population.[2] Patients with articular cartilage damage usually experience pain, inflammation, stiffness of the joints and limited range of motion.[3] Cartilage tissue that has undergone trauma and is left untreated eventually degenerates, leading to the development of chronic osteoarthritis.[4] The absence of innervation and vascularization of articular cartilage, together with its low cell density, are the main factors limiting the self-renewal properties of the tissue and the success of tissue engineering approaches.[5]

Current tissue engineering approaches focus either on analgesic or reconstructive techniques. Analgesic techniques use local administration of drugs such as corticosteroids,[6] hyaluronic acid (HA),[7] or autologous platelet-rich plasma[8] to reduce inflammation and pain, but they do not promote tissue regeneration. On the other hand, reconstructive techniques attempt to repair cartilage lesions by stimulating cells to restore the damaged tissue.[9] Examples of such techniques are microfracture, autologous chondrocyte implantation

E. Tosoratti, P. Fisch, M. Zenobi-Wong
Institute for Biomechanics
Otto-Stern-Weg 7, ETH Zürich, Zürich CH-8093, Switzerland
E-mail: marcy.zenobi@hest.ethz.ch

S. Taylor
Poly-Med Inc
51 Technology Drive
Anderson, SC 29625, USA

L. A. Laurent-Applegate
Regenerative Therapy Unit
Lausanne University Hospital
University of Lausanne
Épalinges CH-1066, Switzerland

L. A. Laurent-Applegate
Center for Applied Biotechnology and Molecular Medicine
University of Zürich
Zürich CH-8057, Switzerland

The ORCID identification number(s) for the author(s) of this article can be found under https://doi.org/10.1002/adhm.202101094

DOI: 10.1002/adhm.202101094

(ACI), and matrix-assisted autologous chondrocyte implantation (MACI).[10]

Hydrogels have gained interest for cartilage tissue reconstruction, as they can mimic the extracellular matrix of many tissues, providing a 3D environment for cells to migrate and proliferate.[11] Their highly swollen and porous nature allows for solutes and nutrients to freely diffuse within, providing a highly biocompatible environment for cell encapsulation.[12] In the last decade, a variety of synthetic and naturally derived hydrogels have been developed and used to generate 3D constructs for cartilage engineering,[13,14] but higher performance has been reported in naturally derived hydrogels in terms of glycosaminoglycans, collagen type II, and aggrecan deposition.[15–17] Specifically, chondrocytes encapsulated in hyaluronan have shown cell proliferation and matrix deposition suitable for the regeneration of cartilage tissue.[18,19]

Various studies[20–24] have shown how hydrogel stiffness and the bioactivity of the embedded cells are inversely correlated, i.e., softer hydrogels allow cells to migrate easily, differentiate better, and to remodel the surrounding matrix faster than stiffer environments. At the same time, hydrogels which are too soft may not be capable of remaining stable under inflammation, skin tension, tissue movements, or once they are implanted and mechanically loaded. In particular, hyaluronan and hyaluronan based hydrogels have shown to be optimal for tissue engineering since hyaluronan is one of the main components of the extracellular matrix,[25] in particular cartilage, where together with proteoglycans it forms aggregates, responsible for the extraordinary mechanical properties of cartilage and has shown to be a crucial component for cell proliferation and migration.[26] Recent works[27–31] have shown the potential of enzymatically crosslinking HA for tissue engineering, where excellent biocompatibility, cell proliferation and tissue maturation can be observed. Furthermore, the enzymatic crosslinking process involves FXIII, a multifunctional protein involved in a variety of mechanisms for regulation and repair processes, such ECM stabilization and wound healing.[32]

Scaffolds such as metals, ceramics, and plastic have been used in combination with soft hydrogels to provide additional mechanical stability.[33–36] In fact, many recent tissue engineering approaches are based on the use of biodegradable polymers and additive manufacturing technologies for the generation of patient-specific scaffolds.[14,37–39] These materials allow for the design of hydrogel-supporting structures that sustain the construct during early implant stages and degrade after a specific amount of time. Among these polymers, synthetic biodegradable poly-lactides such as polycaprolactone (PCL), poly(glycolic acid) (PGA), and polylactic acid (PLA) have been investigated in the last decade, as they possess biocompatible degradation pathways, thermal plasticity,[40] and suitable mechanical properties.[40,41] When implanted, these polymers can degrade through hydrolysis of their ester bonds.[42] The applications for these polymers include dissolvable sutures, implants for fixation of bone, drug delivery, and tissue engineering.[42]

Unfortunately, commonly used degradable polymers possess either very slowly degrading pathways that can take up to several years to be broken down,[43] or very fast-degrading properties that do not provide adequate reinforcement support for the desired amount of time.[44] On one hand, an excessive permanence of the reinforcement structure and an excess of degradation of the byproducts may hinder further cell proliferation and tissue maturation or even lead to cell death.[45,46] On the other hand, a premature degradation may prevent adequate reinforcement and lead to deformation and rupture of the construct.[45,46] Most tissue regeneration approaches and the specific interaction of cells with the different hydrogel materials call for the design and manufacture of specific biodegradable scaffold materials with targeted mechanical and degradation properties. This would enable the generation of constructs with an adequate mechanical stability upon implantation, where the reinforcement structure is designed to degrade once sufficient mechanical stability is provided by the matrix secreted by the cells.

In this work, a novel lactide copolymer termed Lactoprene® 7415 is employed to match the matrix stiffened by human chondroprogenitors in a hyaluronan-based hydrogel for the regeneration of cartilage tissue. Lactoprene® 7415 is a linear segmented block copolymer with an A-B-A structure containing a large central block of trimethylene carbonate with end grafts comprising lactide (74%), trimethylene carbonate (15%), and caprolactone (11%) repeat units. This structure creates a tough, flexible polymer with low crystallinity. Additionally, minimizing the lactide in the polymer matrix minimizes the generation of lactic acid during polymer degradation, and the lower crystallinity reduces the surface hardness of the polymer. With a hydrolysis-based degradation, the construct can be naturally degraded in vitro and in vivo. First, the degradation of the reinforcement copolymer is analyzed in vitro by means of high-performance liquid chromatography (HPLC) over the course of 63 d. Second, the optimized scaffold design is 3D printed using fused deposition modeling (FDM) and embedded in an enzymatically crosslinked hyaluronan hydrogel loaded with human epiphyseal chondroprogenitors (ECPs) for cartilage tissue regeneration. Third, the maturation of the reinforced construct is evaluated over the course of 63 d and compared to the nonreinforced hydrogels. Finally, an in vivo study is performed, illustrating the possibility of implanting these reinforced constructs without a preculture period. Our results suggest that such composites may be used following a 1d preparation in a one-step surgical procedure. This approach may be used thereafter in combination with existing techniques; for instance, with cartilage mincing where cells and tissues from patients do not leave the operating room but are harvested and re-implanted right away with little manipulation by the surgeon, with cells from previously stocked Biobanks (such as with ECPs) or with autologous preparations of chondrocytes.[47,48]

2. Results and Discussion

2.1. Lactide Copolymer Scaffold Design, Degradation Analysis, and HA-TG Hydrogel Embedding

Lactoprene® 7415 (Polymed, Inc), a novel lactide-copolymer, was investigated as a reinforcement material for the regeneration of cartilage tissue. The material is a flexible copolymer comprising 74% l-lactide, 15% trimethylene carbonate, and 11% caprolactone. Scaffolds were designed and 3D printed using Lactoprene® 7415 and a 10% recto-wiggle pattern in the shape of a parallelepiped, from which 6 mm cylinders were cut out and used as a reinforcement material (**Figure 1**A). The recto-wiggle

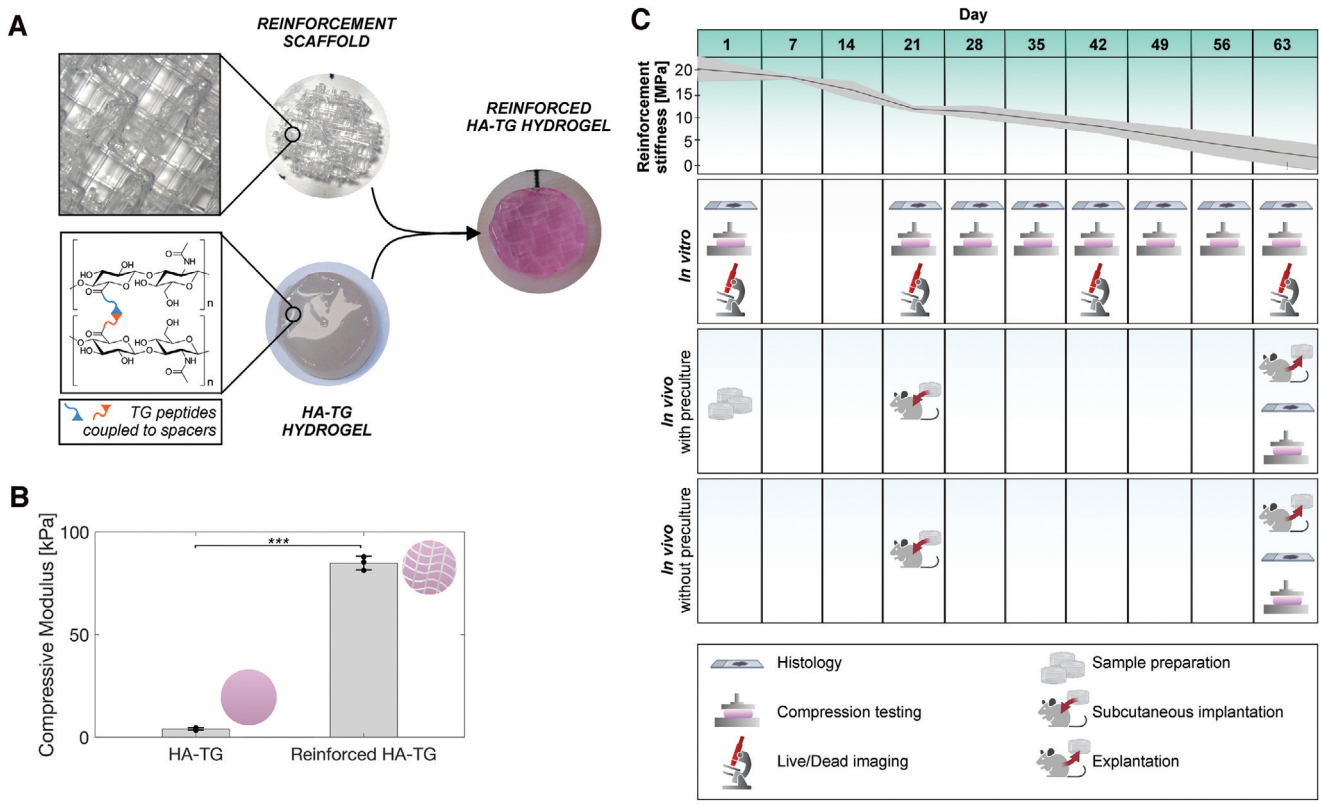

Figure 1. Schematic of components and embedding process. A) Lactoprene® 7415 reinforcement scaffolds were 3D printed using a 10% recto-wiggle infill pattern and were combined with a HA-TG hydrogel to form a reinforced HA-TG. B) Compressive modulus of HA-TG hydrogel alone and in combination with the reinforced scaffold. Data represents mean and standard deviation of $n = 3$ independent experiments. The p value was determined using a simple t-test. C) Experiment timeline; in green: degradation of the lactide reinforcement material over the course of 9 weeks represented by a quasi-linear decrease of the Young's modulus. Shaded in red: an in vitro study allowed for analysis of the material mechanically (compression testing), histologically, and by immunofluorescence (live/dead) at different timepoints. Shaded in blue: in vivo study, samples were prepared and left to preculture for 3 weeks (top row) before being implanted, while another set of samples was prepared and implanted at week 3 (bottom row). In vitro and in vivo analysis were performed at week 9.

pattern was chosen to provide flexibility to the scaffold, while still speeding up the printing process since each layer had a continuous printing path and required only a few turns by the printing head. By minimizing the number of passes, the failure rate of the prints was also greatly reduced. The 3D-printed scaffold was then combined with a 1.5% enzymatically crosslinked hyaluronan transglutaminase (HA-TG) hydrogel previously developed in our laboratory.[30] In this respect, the recto-wiggle pattern provided a larger surface area in contact with the HA-TG hydrogel compared to a simple rectilinear grid, since the curvature of the strands lead to a higher amount of material deposited in the same volume. This also increased the overall stiffness of the scaffolds, without reducing their overall flexibility. At the same time, the recto-wiggle pattern created a more open interconnected pore network which facilitated the injection of HA-TG. The embedded reinforcement structure increased the overall compressive modulus of the hydrogel from 4.1 ± 0.6 to 84.9 ± 3.3 kPa (Figure 1B).

The degradation of Lactoprene® 7415 was analyzed by submerging 3D printed, tensile bar shaped samples (Figure S1, Supporting Information) in PBS. Tensile strength and ultimate tensile strength (UTS) were recorded over the course of 63 d. Figure 1C and Figure S2A (Supporting Information) show the Young's modulus of the reinforcement material, where a linear decrease in tensile strength over time is observed. Specifically, the Young's modulus of the material decreased from 20.5 ± 2.8 to 1.6 ± 2.7 MPa after 63 d. The strength of the material decreased so extensively after 56 d that tensile testing could not be performed on some of the samples at the 63 d timepoint. The decrease in mechanical properties was further confirmed as a tenfold reduction in UTS after 21 d (Figure S2B, Supporting Information).

The mass and the molecular weight loss of the reinforcement material was evaluated using 3D FDM-printed 6 mm cylinders degraded in DMEM media. The degradation was measured via HPLC over the course of 112 d. As can be seen in **Figure 2**A, a steady mass loss of Lactoprene® 7415 samples was observed throughout the experiment. After 112 d, the molecular weight decreased to 36.8 ± 4.0 kDa (Figure 2B), which is nearly a sixth of the value recorded at the start of the experiment (217.7 ± 14.8 kDa).

The degradation profile of the reinforcement revealed excellent properties for use as a degradable scaffold for tissue engineering. The Young's modulus of the scaffold showed sufficient strength over the course of 63 d, where a linear degradation profile was observed (Figure S2A, Supporting Information). This initial high stiffness is beneficial for the sample to maintain its structural

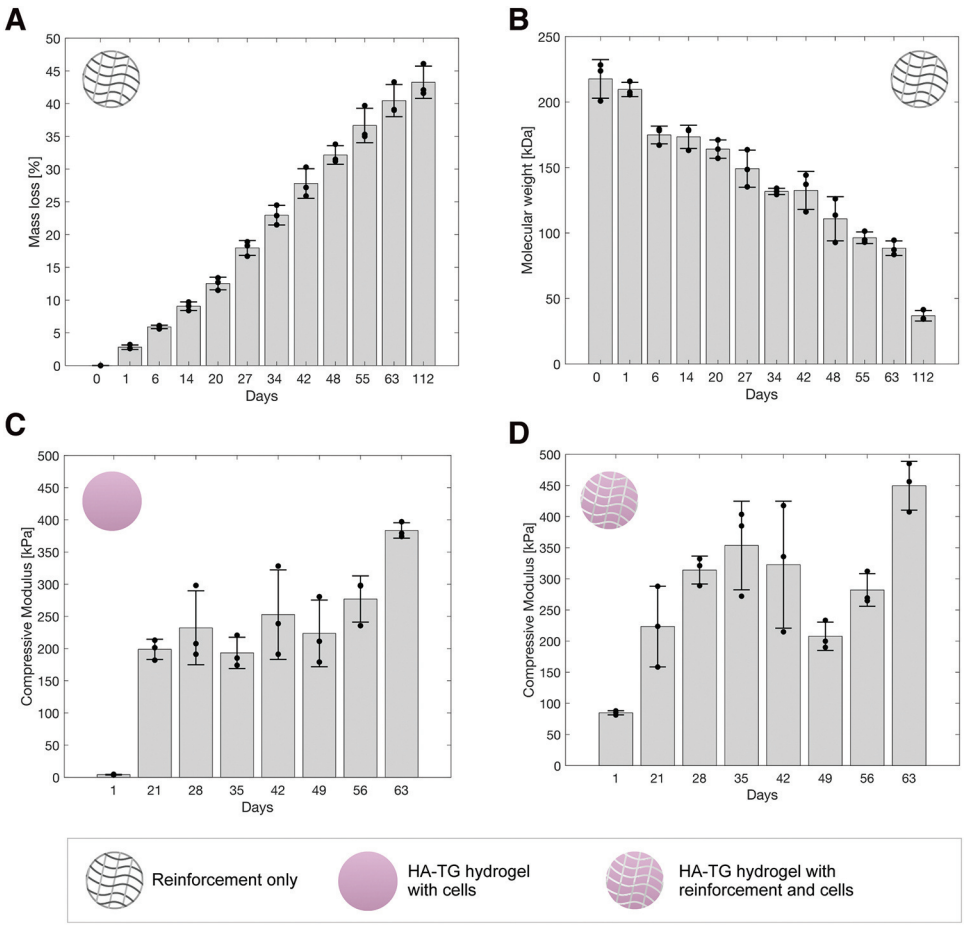

Figure 2. Mechanical testing and degradation of the reinforcement material and of the HA-TG hydrogel. A) The cumulative mass loss of the reinforcement material is shown in percentage over the course of 112 d ($n = 3$). Release of the material was measured via HPLC. Each timepoint was found statistically significant with respect to day 0. B) Molecular weight (Mw) of the reinforced material over the course of 112 d with a quasi-linear downward skewed decrease with a clear drop at day 112 observed. Each timepoint was found statistically significant with respect to day 0, except for day 1. C) Compressive modulus of the HA-TG hydrogel over 63 d ($n = 3$): A first net increase in stiffness was observed between day 1 and day 21, followed by an upward-skewed plateau until day 49 with a final pronounced increase in stiffness at day 63. Each timepoint was found statistically significant with respect to day 1. D) Compressive modulus of the reinforced HA-TG hydrogel over the course of 63 d ($n = 3$): A linear increase in stiffness was observed from day 1 to day 35, followed by a drop in stiffness at day 42. The samples recovered in stiffness after this timepoint, reaching similar values to the HA-TG hydrogel without reinforcement at day 63. Data represents mean and standard deviation of $n = 3$ independent experiments. Each timepoint was found statistically significant with respect to day 1. *P* values were calculated using a simple *t*-test.

integrity, while the soft cell-laden hydrogel promotes matrix deposition by the embedded cells. Once cells have sufficiently stiffened the hydrogel by matrix deposition, the reinforcement structure is no longer necessary and should be entirely replaced by extracellular matrix. Furthermore, the mass loss detected in the DMEM media over the course of 112 d never exceeded 6% of the total weight of the scaffold at any timepoint (Figure S3, Supporting Information). This is an important factor, because sudden spikes in material release may hinder cell proliferation and maturation due to an accumulation of byproducts.[49] Finally, the rate of weight loss of the reinforcement scaffold was found to be steady for the initial 3-week maturation phase (Figure S3, Supporting Information). This is ideal since in this initial phase the reinforcement is needed, as the cells have just started to produce the extracellular matrix and therefore the overall samples are still soft (Figure 2C). As a comparison, other in vitro degraded polymers commonly used in tissue engineering such as PLA and PCL have a much slower degradation time, where less than 4% loss in weight is observed after 42 d[50,51] whereas the Lactoprene® 7415 reinforcement already lost almost 30% of its mass at the same timepoint. PLA and PCL are therefore suboptimal polymers for such applications since they do not degrade fast enough, inhibiting the remodeling process of the cells. At the same time, commonly used PGA has a much faster degradation rate, leading to insufficient mechanical stability and an inability to adequately reinforce the hydrogel.

2.1.1. Cytotoxicity

An MTS assay was performed to evaluate the change in metabolism of cells when exposed to the reinforced material alone in culture media. Figure S4A (Supporting Information) reports the measured absorbance of formazan by cells cultured

with and without a reinforced scaffold, where a higher absorbance signifies higher cell metabolism. A 2.5 times reduction in absorbance was observed when the reinforced material was added to the media solution. The reduction in absorbance suggested a lower metabolic cell activity in presence of the reinforced material. To evaluate if the reduction in absorbance was linked to cytotoxicity, a viability analysis was performed to evaluate the biocompatibility of the Lactoprene® 7415 material over 21 d (Figure S4B,C, Supporting Information) where the scaffold was embedded in a 1.5% HA-TG hydrogel solution. Over the course of 21 d, viability remained above 90% (live cells at day 1: 96.1% ± 2.1%, day 7: 92.9 ± 6.2%, day 21: 95.0% ± 1.5%).

The MTS assay is considered one of the "gold standards"[52,53] for the cytotoxicity evaluation of a material. It allows for the determination of cell metabolic activity change as the potential for cells to metabolically reduce MTT into formazan.[54] Nevertheless, the results of an MTS assay should always be carefully interpreted as they may be affected by a variety of factors, such as small fluctuations in pH of medium, reduction of the tetrazolium salts or simply from initial byproducts of reinforced material.[52,54] For this reason, a viability test was performed to evaluate the viability of cells in the presence of the reinforcement material once embedded in a HA-TG hydrogel. Since previous studies have shown that HA-TG is an excellent hydrogel for cartilage regeneration,[27–31] any reduction in viability would be linked to the presence of the reinforcement material alone. A viability analysis was performed to evaluate the biocompatibility of the reinforcement structure when combined with the HA-TG hydrogel over 21 d (Figure S4B,C, Supporting Information). Results showed excellent viability and proliferation of cells (Figure S4C,D, Supporting Information), as could be seen from the two-fold increase in cell number at day 7 and the fivefold increase at day 21. These results confirmed the biocompatibility of the reinforced material and ensured that the decrease in metabolic activity of the MTS assay was not related to increased cytotoxicity.

2.2. In Vitro Maturation and Mechanical Testing of HA-TG Hydrogels and HA-TG Reinforced Hydrogels

Once the biocompatibility of the reinforcement material was established, the reinforcement structure was embedded in 1.5% HA-TG together with human ECPs (10 million mL^{-1}). As a control, chondroprogenitors were also encapsulated in an HA-TG hydrogel. Compression testing was performed to evaluate the change in compressive modulus of the two conditions over time. Figure 2C reports the compressive modulus of 6 mm diameter, 1.5 mm thick HA-TG samples cultured in chondrogenic media over the course of 63 d. A significant increase in stiffness ($p < 0.001$) was observed between day 1 and day 21, followed by a positively skewed maturation plateau until day 49. Finally, a second substantial stiffness increase was observed between day 49 and day 63, when samples reached a final compressive modulus of 383.4 ± 12.0 kPa.

The addition of the reinforced scaffold resulted in an increased compressive modulus at day 1 of 84.9 ±3.3 kPa with respect to an initial 4.1 ± 0.6 kPa of the HA-TG hydrogel alone. The reinforcement provided structural support up to day 35 (Figure 2D). Between days 42 and 49, the overall mechanical stiffness of the reinforced samples decreased but regained compressive modulus at day 56, reaching similar values to those of the HA-TG samples of Figure 2C.

Previous studies,[27–31] reported a significant maturation of the HA-TG hydrogels in the first three weeks of culture due to the deposition of ECM from the cells leading to an increase in overall stiffness of the samples. Nevertheless, the very low stiffness of the HA-TG hydrogel reported at day one implies that implantation at this early stage could be at risk of failure. In fact, the soft samples may be easily deformed by skin tension, tissue inflammation or body movements. The addition of the reinforced material increased the initial compressive modulus to a value that allows for easier manipulation of the samples and provides the samples with extra strength to sustain skin tension once implanted.

By comparing the degradation profiles in Figure 2A,B, it is possible to deduce that a significant amount of the Lactoprene® 7415 degraded between days 42 and 49. Considering the cumulative mass loss up to day 42, the reinforced structures had an average 30.7% mass decrease with respect to their initial value. Literature reports a similar behavior for hydrolytically degraded copolymers, where the degradation rate of a scaffold can be delayed to a specific timepoint by modifying the molecular chains of the copolymer.[55,56] In the case of Lactoprene® 7415, there is a clear increase in degradation byproducts between day 20 and day 27 (Figure S3, Supporting Information). With respect to the pure HA-TG samples, reinforced HA-TG samples dropped in stiffness between day 42 and day 49. This strong degradation was also empirically observed as the layers of the scaffold could be separated upon gentle mechanical stimulation using forceps at day 42. This phenomenon can be explained by considering the hydrolytic degradation process of the reinforcement material, where most of the degradation occurs on the surface of the scaffold.[57] In particular, a decrease in the stability of the scaffolds occurred due to the small contact area between the layers which degraded first. As the connections degrade, the stiffness provided by the scaffold diminishes, leading to a loss of the compressive modulus. During this degradation process, cells continue to deposit extracellular matrix and thereby to stiffen the surrounding hydrogel. Between day 49 and day 63, the effects of the softening of the reinforcement due to the degradation are outbalanced by the stiffening of the hydrogel due to extracellular matrix deposition, leading to an overall increase in stiffness of the samples. The large standard deviation at day 42 of Figure 2D may be explained by differences in the degradation onset of the reinforced material replicates and by the consideration of differences between the samples due to the FDM printing process. The consequent increase in stiffness observed for the last two timepoints signifies that cells are alive and proliferating, so that the previous decrease in stiffness can be attributed to the degradation of the scaffold exclusively and not to cell death. Finally, this shows that cells embedded in the reinforced samples can remodel the surrounding hydrogel, reaching similar stiffness values to those of the HA-TG hydrogels alone. This implies that by the 63 day timepoint, the scaffold has degraded to the extent where its stiffness can be considered negligible compared to the matrix deposited by the cells. The properties of the scaffold are highly affected by its porosity. On one hand, a higher porosity would lead to a more

compliant scaffold and faster weakening of its macroscopic properties. On the other hand, printing with a greater infill would decrease the porosity leading to a more stable scaffold with a higher number of connection points between the printed strands.

2.3. Viability and Chondrogenesis of ECPs in HA-TG Hydrogels and Reinforced HA-TG Hydrogels

The biocompatibility of the HA-TG hydrogel alone and of the reinforced HA-TG construct was assessed in vitro by means of viability staining and immunohistological stainings. Viability images (**Figure 3**A) were acquired at four timepoints throughout the experiment using a two-photon microscope (Leica Sp8 MultiPhoton). Viability remained above 90% over the course of 63 d (Figure S4E, Supporting Information). At day 1, cells showed a rounded shape and a low density (Figure 3A). At day 21, the morphology of the cells changed to an elongated shape, while their density increased substantially. Figure 3A also shows the deposition of collagen fibers (depicted in blue), through a process known as second-harmonic, characteristic of two-photon imaging.[58] Specifically, these fibers were often found concentrated around the reinforced scaffold at day 42 showing a preferential alignment along the longitudinal direction of the reinforcement strands. No difference in cell morphology or proliferation was observed between the HA-TG-only and the reinforced samples, but cells and their secreted collagen were observed in close contact with the lactide reinforcement. Furthermore, Figure 3B shows an increase in intensity of the colorimetric staining, which indicates that collagen and glycosaminoglycan production increased over time and localized around the reinforced scaffold (Figure 2C). Semiquantitative analysis of the histological and immunohistochemical images showed an increase in intensity of glycosaminoglycans, collagen I and collagen II over the 63 day culture period (Figure S5A, Supporting Information).

The viability study not only allowed for the analysis of cell viability in the two different conditions, but also allowed to gain insights into the morphogenesis and proliferation within the HA-TG hydrogel. In particular, we observed how the morphology of the chondrocytes was altered from a rounded shape on day 1 into a more elongated shape on day 21 with a significant amount of collagen fibers being deposited. As reported in the literature,[59] collagen deposition was found concentrated around the fibers, further confirming the biocompatibility of the reinforcement material. Furthermore, proliferation was seen as cells began to replicate and move to less densely populated regions of the hydrogel. The viability of cells was also uniform across the sample, showing good diffusion of nutrients and gasses. In addition, the histological analysis conducted at different timepoints allowed for assessment of maturation and matrix deposition of the samples over time. Glycosaminoglycan production (Safranin O staining) was constant over time with no difference between the reinforced and nonreinforced samples. At the same time, a steady increase in collagen production could be observed for both conditions over time. Collagen I is uniform in intensity across the whole sample, while collagen II deposition has higher intensity in the central part of the samples. Again, no significant difference can be observed between the two conditions. Collagen I and Collagen II deposition is also observed in contact with the scaffold structure (Figure 3D), signifying that the degradation byproducts do not interfere with matrix deposition by the cells.

2.4. In Vivo Implantation

To confirm the stability and maturation results observed in the in vitro study, an in vivo study was performed in which reinforced HA-TG samples were implanted subcutaneously in nude mice. Half of the implanted samples were precultured for 21 d prior to the implantation, while the remaining half was prepared fresh on the day of surgery (Figure 1B). The samples were explanted after 42 d, and they all retained their shapes and could be seen under the skin of the mice (**Figure 4**A). As expected, precultured samples had higher compressive moduli compared to non-precultured samples, since they were cultured for 3 additional weeks in vitro (Figure 4B). Statistical analysis revealed a significant difference with value of $p = 0.002$. Nevertheless, the measured stiffness of 182.3 ± 21.4 kPa for the precultured samples was lower than the expected value of 449.6 ± 39.2 observed in the in vitro study at the 63 d timepoint. Instead, these values appear similar to the stiffness observed at the 49 d timepoint (207.7 ± 22.7 kPa). The difference in stiffness may be attributed to the different dynamics between in vitro and in vivo, where the Lactoprene® 7415 scaffold may have been degraded more rapidly or where cells may have developed at a slower rate. This phenomenon has been previously reported in the literature, where the animal metabolism increases the rapidity of degradation of the scaffold upon reabsorption processes.[60] Finally, the histological analysis (Figure 4C) shows good glycosaminoglycan and collagen production, but the Collagen I to Collagen II ratio is higher than in the in vitro results. Precultured samples showed a higher intensity of glycosaminoglycans ($p = 0.06$), a significant increase in collagen II intensity ($p = 0.01$) and a significant decrease in Collagen I intensity ($p = 0.03$) compared to non-precultured samples (Figure S5B, Supporting Information).

Subcutaneous implantation in mouse models is a commonly used procedure for evaluating the biocompatibility of a graft[61] and for evaluating the development of chondrocytes in vivo for cartilage regeneration.[62] In addition to an upregulation in the degradation of the scaffold material due to the increased turnover by the host, the increased amount of oxygen found in the subcutaneous environment of the animal may have hindered the growth of chondrocytes.[63] Furthermore, the in vitro samples were cultured using chondrogenic media (supplemented with TGFβ3), which upregulates the maturation and matrix production of chondrocytes. On one hand, the lower intensity of the Safranin O staining in the in vivo study may indicate a slower maturation of the chondrocytes compared to the in vitro results (Figure 3C, Figure S5B, Supporting Information). On the other hand, the upregulation of Collagen I deposition in conjunction with the downregulation of Collagen II production may be linked to cell dedifferentiation and loss of the chondrogenic phenotype.[64] Finally, a small capsule was found around the samples, but no vascularization was observed within the samples (Figure 4D).

Alternatively, the presented approach may also be used in a one-step procedure for second-generation autologous cartilage repair techniques.[65,66] With this technique, a small cartilage

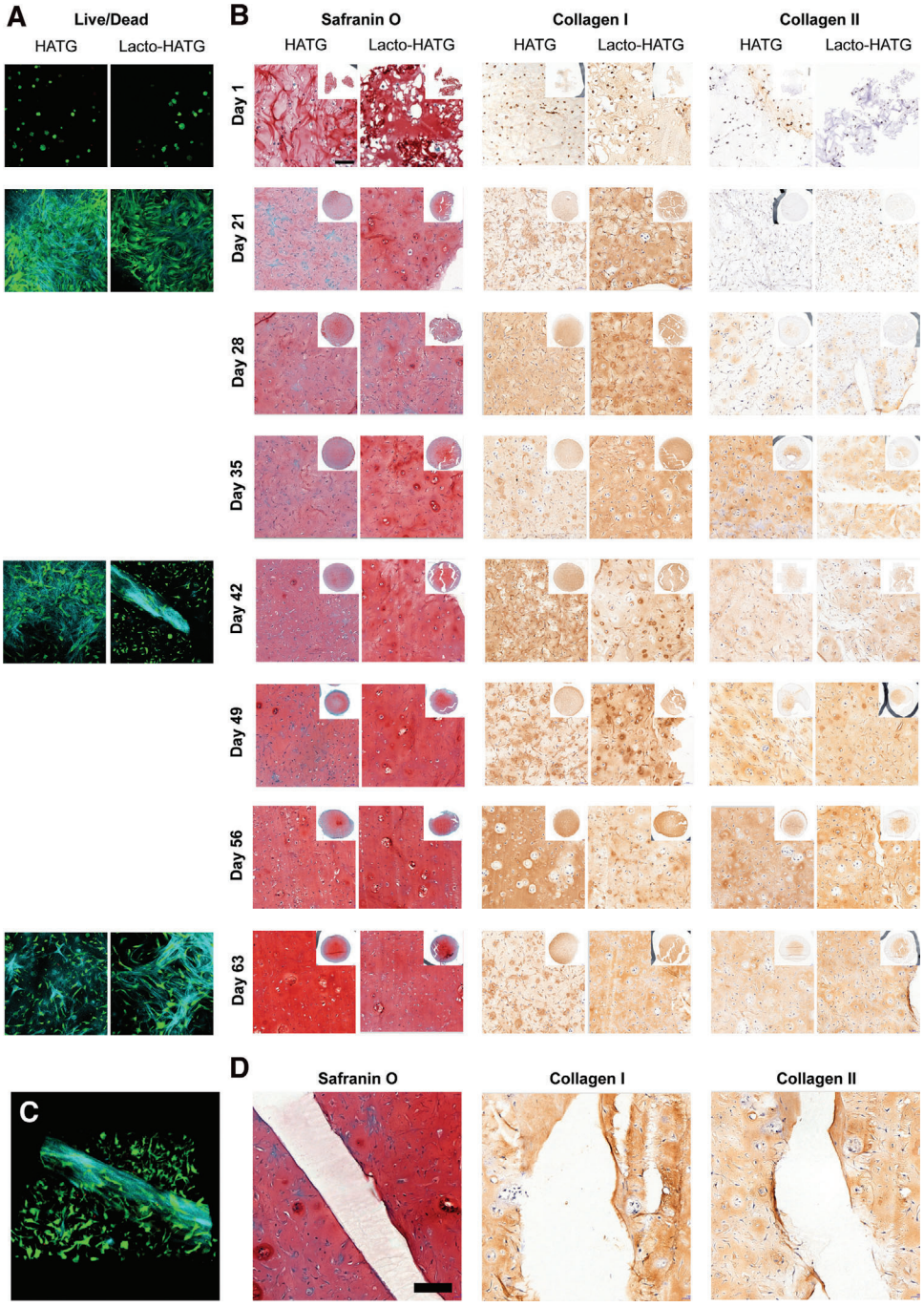

Figure 3. Live/dead and histological analysis of HA-TG and reinforced HA-TG samples. A) Live/dead immunofluorescence was performed using a 2-photon microscope. At day 1, cells were round in shape and sparse in number. From day 21, proliferation and spreading of cells was evident. Second harmonic generation allowed to observe collagen fiber deposition (blue). Cells continued to proliferate and spread over the course of the entire experiment. B) Histological analysis showing glycosaminoglycans (Safranin O), Collagen I and Collagen II deposition over the course of 63 d. No significant difference could be observed between the HA-TG and the reinforced HA-TG samples, in which cells continued to deposit matrix. The reinforced scaffold did not interfere with the deposition of matrix. C) 3D-view of the collagen deposition by cells at day 42. D) Deposition of matrix near the reinforced structure has an even transition, with no difference with respect to the rest of the gel. Cells remain alive and unaffected by the presence of the reinforced transition zone.

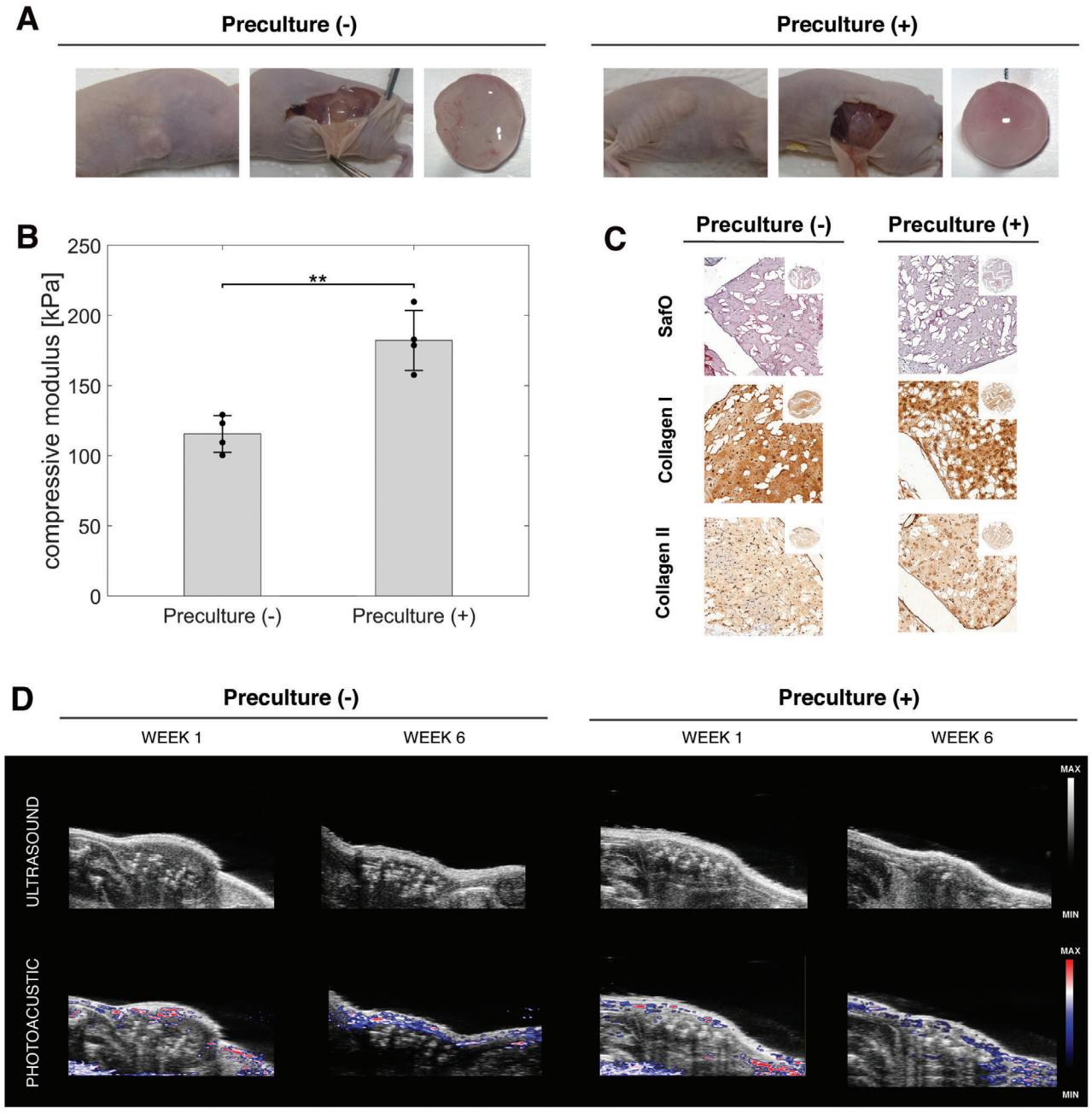

Figure 4. In vivo implantation. A) Pictures showing the samples after subcutaneous implantation, without preculture and with 21 d of preculture. B) Compressive modulus of the samples without and with preculture. Data represents mean and standard deviation of $n = 3$ independent experiments. The p-value was determined using a simple t-test. C) Histological analysis of the in vivo samples. D) Ultrasound and photoacoustic of the samples at day 63 to confirm the absence of vascularization within the samples.

defect is generated from a non-load-bearing region of the patient knee and is minced to generate small cartilage fragments. These tissue fragments contain chondrocytes that, once embedded in a hydrogel, can migrate into the surrounding biomaterial and produce extracellular matrix.[66] These small tissue fragments may be combined with the HA-TG and Lactoprene® 7415 reinforced composite described in this work to be reimplanted immediately, without the need of a second surgical procedure.

3. Conclusion

By analyzing the maturation profile of biological materials, it is possible to develop reinforced structures with specific biodegradation properties. This permits the development of composite structures with a predetermined compressive modulus capable of sustaining pressure, skin tension and body movement at the time of implantation, leading to better tissue regeneration and

a lower risk of implant failure. At the same time, these scaffolds can be tuned to degrade when the bulk hydrogel material has been successfully remodeled by the embedded cells. This avoids having the scaffold material in place for a longer period than required. The combination of the HA-TG hydrogel with a Lactoprene® 7415 reinforced structure allowed for the successful promotion of the regeneration of cartilage in both in vitro and in vivo settings, where excellent proliferation and matrix production could be observed. In the case of the in vivo experiment, our approach allowed us to validate the possibility of implanting reinforced samples with no need of a preculture period, achieving identical outcomes in terms of shape fidelity and tissue maturation compared to HA-TG samples alone. It is therefore possible that by limiting cell manipulation (no cell culture delay imposed) and re-implanting patient cells immediately in a one-step operation, regulatory pathways could effectively be shortened and patients would have effective therapies available rapidly.

4. Experimental Section

Chemicals: All chemicals were purchased from Merck unless otherwise stated.

Cell Source and Expansion: ECPs were isolated as previously described from the proximal ulnar epiphysis of a 14-week gestation donor.[67] ECPs were seeded at 10 000 cells cm^{-2} in standard tissue culture plastics (Nunc) in Dulbecco's Modified Eagle's Medium (DMEM 41966, Sigma-Aldrich) supplemented with 10% v/v FBS, 10 µg mL^{-1} gentamicin and 50 µg mL^{-1} L-ascorbate-2-phosphate at 37 °C, 5% CO_2 and 95% humidity. ECPs were passaged after 8 d at 80% confluency following two media changes and used at passage 3 for gel preparation. Approval of the experimental protocols was received from the Ethics Committee of the canton Vaud (CHUV—Centre Hospitalier Universitaire Vaudois of the Vaud) and experiments performed under the protocol 62/07.

HA-TG Synthesis: HA-TG was synthesized as previously described.[30] Briefly, thiolation of HA was carried out by coupling 3,3'-dithiobis(propanoic dihydrazide) (DTPHY) via 1-Ethyl-3-(3-dimethylaminopropyl)carbodiimide and afterwards reducing DTPHY by the addition of tris(2-carboxyethyl)phosphine hydrochloride. The product was dialyzed against ultrapure water adjusted to pH 4.5. Subsequently divinylsulfone was coupled to DTPHY via Michael Addition and the product dialyzed against ultrapure water. Lastly the solution was split into two parts and substituted with either the lysine donor peptide (FKGG-ERCG, TG/K) or the glutamine donor peptide (NQEQVSPL-ERCG, TG/Q). Following HATG/Q/K was dialyzed again against ultrapure water, filtered through a 0.45 µm filter and lyophilized. A degree of substitution of ≈10% over the disaccharide repeating units was confirmed by 1H-NMR.

Sample Preparation and Culture: Cells were embedded at a concentration of 10 million cells mL^{-1} in 1.5% HA-TG. The viability before encapsulation was measured by trypan blue exclusion on a Countess device (Thermo). Gelation was achieved as described by Broguiere et al.[30] Briefly, the gel precursors were suspended at 1.5% w/v in sterile TBS (NaCl 150×10^{-3} M, $CaCl_2$ 50×10^{-3} M, TRIS 50×10^{-3} M, pH 7.6). Crosslinking was initiated by adding 12.5 U mL^{-1} thrombin (Baxter) and 10 U mL^{-1} factor XIII (Fibrogammin, CSL Behring). Gels were cast in sterilized PDMS (SYLGARD 184) molds of 6 mm diameter and 1.5 mm height placed in the well plate. To generate reinforced samples, the reinforcement material was pressed on top of the casted samples to avoid air bubble formation within the sample. Gels were left to crosslink for 15 min at 37 °C and chondrogenic medium was then added. After one day, the PDMS molds were lifted to allow the gels to float freely. Samples were cultured in 12-well plates with DMEM supplemented with 10 ng mL^{-1} transforming growth factor $\beta 3$ (TGF-$\beta 3$, Peprotech), 50 µg mL^{-1} L-ascorbate-2-phosphate, 40 µg mL^{-1} L-proline, 50 µg mL^{-1} gentamicin (Gibco) and 1% ITS+ Premix (Corning). The well plates were placed in tissue culture incubators at 37 °C and 5% CO_2. Cultures were maintained for up to 63 d and media changes performed twice a week.

Lactoprene® 7415 Synthesis: Lactoprene® 7415 was fabricated by ring opening polymerization with stannous octoate as a catalyst. The polymer was ground with a Wiley mill and purified by devolitalization using a Heidolph rotoevaporator. This purified polymer was extruded using a custom ¾" single barrel extruder (Alex James & Associates, SC, USA) into a monofilament with 1.75mm nominal diameter. The overall polymer composition is 74% lactide, 15% trimethylene carbonate, and 11% caprolactone.

Lactoprene® 7415 Sample Manufacture: A lactide copolymer (PolyMed, Inc, Anderson SC, USA) was 3D printed using a 10% recto-wiggle in the shape of a 20 cm by 20 cm rectangular parallelepiped with the layer printing direction rotated by 90° every two layers. Cylinders with a diameter of 6 mm were then cut out using a metal puncher heated to 100 °C (Figure 1A, Figure S6, Supporting Information). A F306 printer (Fusion3) was used for the manufacturing process with a bed temperature of 100 °C and a nozzle temperature of 180°. Printing was performed using a 0.15 mm nozzle diameter and a 0.075 mm layer height at 250 mm min^{-1}. Before use with cells, the 3D-printed samples were immersed for 30 min in a 70% EtOH solution, dried in a sterile environment and UV sterilized for 30 min. Samples were imaged using a Leica M650 microscope (Figure S6A, Supporting Information). To calculate the porosity of the scaffolds, layers were separated (Figure S6B, Supporting Information) and the ratio of void space to the ratio of material was calculated as described in literature.[68] The overall mean porosity was found to be 91.0% ± 3.11%, as expected by the 10% infill pattern used in the printing process.

Lactoprene® 7415 Degradation Analysis: A set of the same 3D-printed 6 mm cylinders used for the in vitro and in vivo studies was used to analyze the degradation of the lactide material over the course of 112 d. Triplicates were immerged in a DMEM (Gibco DMEM, High Glucose, GlutaMAX Supplement, Pyruvate, from Fisher Scientific) buffer solution with 50 µg mL^{-1} ascorbic acid (BioXtra, from Millipore Sigma). Specimens were weighed using a 5-digit balance (Mettler Toledo). 20 mL buffer was added to each vial containing a sample and was placed in a 37 °C incubator on an orbiting shaker at 100 rpm. The buffer solution was replaced every 2 to 3 d throughout the study. At each timepoint, samples were removed from the buffer, rinsed in deionized water and dried under reduced pressure to a constant mass in accordance with ASTM F1635. Dried samples were further evaluated for molecular weight by gel permeation chromatography (GPC, Waters Corp.) using dichloromethane as the mobile phase and compared against polystyrene standards. Dried samples were also evaluated for thermal profile by differential scanning calorimetry (DSC, Perkin-Elmer) from 20 to 220 °C at 10 °C min^{-1}.

Tensile Strength Loss Studies were performed on 3D-printed tensile bars (ASTM D638 Type V, made with ½ thickness) manufactured with two outlines and a 100% rectilinear infill at ±30° angle on alternating layers for the tensile testing over the course of 63 d (Figure S1, Supporting Information). The tensile bars were individually submerged in a 100×10^{-3} M phosphate buffer at pH 7.4. Samples were placed at 37 °C and at the predetermined timepoints, removed for mechanical testing and immediately tested. Testing was performed on an MTS Synergie load frame with a 25.4 mm gage length at a speed of 10 mm min^{-1}.

MTS Assay: ECPs were seeded at 10 000 cells cm^{-2} in a 6-well plate. For the untreated control, cells were cultured in phenol-red free DMEM medium supplemented with TGF-ß3 for 2 d. For the vehicle control, lactide scaffolds were placed in the wells on top of the seeded cells for 2 d. Phenol-red free DMEM medium supplemented with 10% of MTS reagent solution (Abcam) was used to perform the MTS assay. A plate reader (Synergy H1, BioTek Instrument) was used to read the absorbance at 40 nm after 30 min.

Subcutaneous Implantation: Animal studies were performed in compliance with the ethical license of the Canton of Zurich Veterinary Office (No. ZH189/2014). Nude mice were obtained from Charles River Laboratories. All animals were female with an age of 17 weeks and a weight of

22.53 g ± 1.45 g. Animals were housed in groups of 4 and allowed to move without restrictions. Standard food and water were provided ad libitum. Two different conditions were investigated in vivo: 1) HA-TG-reinforced samples prepared the day of implantation, 2) 21 d precultured HA-TG-reinforced samples. Mice anesthetization was achieved using 4.5% isoflurane. Meloxicam at a 2 mg kg^{-1} concentration was administered before surgery via subcutaneous injection. Desiccation of corneas was prevented by administering eye cream. Anaesthesia was maintained using 2% isoflurane. Samples were placed subcutaneously via two incisions performed laterally to the dorsal midline at the level of the hips. 3M surgical staples were used to close the incisions. Staples were removed after 1 week. Euthanasia was performed at the end of the experiment via CO_2 asphyxiation. The explanted samples were fixed in 4% paraformaldehyde for 4 h.

Histology and Immunohistochemistry: Samples were dehydrated and paraffin embedded. A microtome was used to cut 5 µm sections of the embedded samples. Safranin-O stainings were performed using standard protocols. Collagen 1 and collagen 2 stainings were performed by digesting the samples in 0.2% w/v hyaluronidase at 37 °C and blocking for 1 h 1:1500 diluted rabbit anti-collagen 1 (Abcam ab138492) and 1:200 diluted rabbit anti-collagen 2 (Rockland Ab) antibodies diluted in 5% normal goat serum. An automated digital slide scanner (Panoramic 250 Flash III, 3D Histotech) was used to achieve uniform exposure and light intensity while acquiring stained slides.

Semiquantitative Evaluation: Semiquantitative evaluation of the histological and immunohistological staining was performed as previously described.[27] Briefly, images were decomposed in channels in ImageJ (National Institutes of Health, USA, v1.52n) using color deconvolution. The channels represented the hematoxylin and DAB stain for Collagen I and Collagen II, while the hematoxylin and stain of glycosaminoglycans for the SafraninO staining. A prebuild framework in ImageJ was used to generate a "H-DAB" vector containing two colors, the first of which represented the hematoxylin-stained nuclei and the second the collagens. Similarly, a vector was built for the Safranin O stain, where the first color represented the hematoxylin-stained nuclei while the second the glycosaminoglycans. The grey mean value of the image was then calculated for each color to extrapolate the intensity of the stain.

Mechanical Testing: Unconfined compression was performed using a Ta.XTplus Texture Analyser (Stable Microsystems) using a 50 N load cell. For the explanted samples, fibrous tissue was carefully removed before compression. All samples were compressed to 15% strain at a rate of 0.01 mm s^{-1} after application of a small preload to ensure proper contact. The slope in the linear range of the stress-strain curve was used to calculate the compressive modulus.

Cytocompatibility: Live/dead imaging was performed at days 1, 21, 42, and 63 using 1 µg mL^{-1} of calcein-AM (Sigma), and 10 µg mL^{-1} Propidium iodide (Fluka) imaged on a Leica SP8 multiphoton microscope.

Ultrasound and Photoacoustic Imaging: Ultrasound and photoacoustic imaging were performed to visualize oxygen saturation surrounding the implants using a Vevo LAZR (*Visualsonics*) system with a LZ550 transducer. Imaging was performed 1 week after implantation and on the day of euthanasia. Hemoglobin content was visualized by exciting underlying tissues around the samples using 700 nm laser pulses. A dual wavelength of 750 and 850 nm was used in conjunction with an Oxyhemo algorithm to assess oxygen saturation.

Statistical Analysis: Statistical analysis was performed on Prism (v 8.02.263, GraphPad) using a simple t-test. A *p*-value below 0.05 was considered statistically significant ($*p < 0.05$, $**p < 0.005$, $***p < 0.001$). Live/dead results were acquired by analyzing three samples per timepoint and three different locations. Compression samples were acquired by analyzing three samples per timepoint. Mean ± standard deviation is reported for all data acquired.

Supporting Information

Supporting Information is available from the Wiley Online Library or from the author.

Acknowledgements

E.T. and P.F. contributed equally to this work.

Open access funding provided by Eidgenossische Technische Hochschule Zurich.

Conflict of Interest

S.T. is an employee of Polymed Inc.

Data Availability Statement

The data are available in the repository of the ETH data collection, doi:0.3929/ethz-b-000483107.

Keywords

3D-printing, cartilage engineering, enzymatically crosslinked hydrogels, hybrid reinforcement scaffolds, lactide-copolymers

Received: June 4, 2021
Revised: September 20, 2021
Published online: October 18, 2021

[1] G. Jiménez, J. Cobo-Molinos, C. Antich, E. López-Ruiz, in *Osteochondral Tissue Engineering: Challenges, Current Strategies, and Technological Advances*, (Eds: J. M. Oliveira, S. Pina, R. L. Reis, J. San Roman), Springer International Publishing, Cham **2018**, pp. 63–83.
[2] E. Thomas, G. Peat, P. Croft, *Rheumatology* **2013**, *53*, 338.
[3] R. F. Loeser, S. R. Goldring, C. R. Scanzello, M. B. Goldring, *Arthritis Rheum.* **2012**, *64*, 1697.
[4] W. C. Bae, M. M. Payanal, A. C. Chen, N. D. Hsieh-Bonassera, B. L. Ballard, M. K. Lotz, R. D. Coutts, W. D. Bugbee, R. L. Sah, *Cartilage* **2010**, *1*, 10.
[5] J. W.-P. Michael, K. U. Schlüter-Brust, P. Eysel, *Dtsch. Arzteblatt Int.* **2010**, *107*, 152.
[6] M. W. Grol, B. H. Lee, *Curr. Opin. Pharmacol.* **2018**, *40*, 59.
[7] Z. Zhu, Y.-M. Wang, J. Yang, X.-S. Luo, *Plast. Aesthetic Res.* **2017**, *4*, 219.
[8] M. I. Kennedy, K. Whitney, T. Evans, R. F. LaPrade, *Curr. Rev. Musculoskeletal Med.* **2018**, *11*, 573.
[9] A. M. Haleem, C. R. Chu, *Oper. Tech. Orthop.* **2010**, *20*, 76.
[10] E. A. Makris, A. H. Gomoll, K. N. Malizos, J. C. Hu, K. A. Athanasiou, *Nat. Rev. Rheumatol.* **2015**, *11*, 21.
[11] B. Balakrishnan, R. Banerjee, *Chem. Rev.* **2011**, *111*, 4453.
[12] S. R. Caliari, J. A. Burdick, *Nat. Methods* **2016**, *13*, 405.
[13] J. Li, G. Chen, X. Xu, P. Abdou, Q. Jiang, D. Shi, Z. Gu, *Regener. Biomater.* **2019**, *6*, 129.
[14] E.-Y. Chuang, C.-W. Chiang, P.-C. Wong, C.-H. Chen, *Adv. Mater. Sci. Eng.* **2018**, *2018*, 4368910.
[15] T. J. Klein, S. C. Rizzi, K. Schrobback, J. C. Reichert, J. E. Jeon, R. W. Crawford, D. W. Hutmacher, *Soft Matter* **2010**, *6*, 5175.
[16] S. Nishimoto, M. Takagi, S. Wakitani, T. Nihira, T. Yoshida, *J. Biosci. Bioeng.* **2005**, *100*, 123.
[17] P. B. Malafaya, G. A. Silva, R. L. Reis, *Adv. Drug Delivery Rev.* **2007**, *59*, 207.
[18] S. A. Unterman, M. Gibson, J. H. Lee, J. Crist, T. Chansakul, E. C. Yang, J. H. Elisseeff, *Tissue Eng., Part A* **2012**, *18*, 2497.
[19] I. L. Kim, S. Khetan, B. M. Baker, C. S. Chen, J. A. Burdick, *Biomaterials* **2013**, *34*, 5571.

[20] G. Huang, l. Wang, S. Wang, Y. Han, J. Wu, Q. C. Zhang, F. Xu, T. Lu, *Biofabrication* **2012**, *4*, 042001.
[21] F. Xu, F. Inci, O. Mullick, U. A. Gurkan, Y. Sung, D. Kavaz, B. Li, E. B. Denkbas, U. Demirci, *ACS Nano* **2012**, *6*, 6640.
[22] D. Hanjaya-Putra, K. T. Wong, K. Hirotsu, S. Khetan, J. A. Burdick, S. Gerecht, *Biomaterials* **2012**, *33*, 6123.
[23] G. D. Nicodemus, S. J. Bryant, *Tissue Eng., Part B* **2008**, *14*, 149.
[24] L. J. Schley, B. Loy, D. Lind, C. Hobot, R. Sparer, D. Untereker, *Biomacromolecules* **2007**, *8*, 2301.
[25] M. N. Collins, C. Birkinshaw, *Carbohydr. Polym.* **2013**, *92*, 1262.
[26] M. Hemshekhar, R. M. Thushara, S. Chandranayaka, L. S. Sherman, K. Kemparaju, K. S. Girish, *Int. J. Biol. Macromol.* **2016**, *86*, 917.
[27] P. Fisch, N. Broguiere, S. Finkielsztein, T. Linder, M. Zenobi-Wong, *Adv. Funct. Mater.* **2021**, *31*, 2008261.
[28] N. Broguiere, F. A. Formica, G. Barreto, M. Zenobi-Wong, *Acta Biomater.* **2018**, *77*, 182.
[29] N. Broguiere, E. Cavalli, G. M. Salzmann, L. A. Applegate, M. Zenobi-Wong, *ACS Biomater. Sci. Eng.* **2016**, *2*, 2176.
[30] N. Broguiere, L. Isenmann, M. Zenobi-Wong, *Biomaterials* **2016**, *99*, 47.
[31] E. Cavalli, P. Fisch, F. A. Formica, R. Gareus, T. Linder, L. A. Applegate, M. Zenobi-Wong, *J. Immunol. Regener. Med.* **2018**, *2*, 36.
[32] V. Schroeder, H. P. Kohler, *J. Thromb. Haemostasis* **2013**, *11*, 234.
[33] P. Diloksumpan, M. de Ruijter, M. Castilho, U. Gbureck, T. Vermonden, P. van Weeren, J. Malda, R. Levato, *Biofabrication* **2020**, *12*, 025014.
[34] Y. Jiang, Y. Yang, X. Zheng, Y. Yi, X. Chen, Y. Li, D. Sun, L. Zhang, *NPG Asia Mater.* **2020**, *12*, 18.
[35] J. Feng, J. Fu, Z. Lin, C. Shang, B. Li, *Visual Comput. Ind. Biomed. Art* **2018**, *1*, 5.
[36] W. Li, X. Liu, Z. Deng, Y. Chen, Q. Yu, W. Tang, T. L. Sun, Y. S. Zhang, K. Yue, *Adv. Mater.* **2019**, *31*, 1904732.
[37] Z. Meng, J. He, Z. Cai, F. Wang, J. Zhang, L. Wang, R. Ling, D. Li, *Mater. Des.* **2020**, *189*, 108508.
[38] D. Hong, D.-T. Chou, O. I. Velikokhatnyi, A. Roy, B. Lee, I. Swink, I. Issaev, H. A. Kuhn, P. N. Kumta, *Acta Biomater.* **2016**, *45*, 375.
[39] X. Yin, L. Jiang, J. Yang, L. Cao, J. Dong, *Biotechnol. Lett.* **2017**, *39*, 1433.
[40] P. d. P. Dias, M. A. Chinelatto, *J. Renewable. Mater.* **2019**, *7*, 129.
[41] J. R. G. Carvalho, G. Conde, M. L. Antonioli, P. P. Dias, R. O. Vasconcelos, S. R. Taboga, P. A. Canola, M. A. Chinelatto, G. T. Pereira, G. C. Ferraz, *Polym. J.* **2020**, *52*, 629.
[42] I. Manavitehrani, A. Fathi, H. Badr, S. Daly, A. Negahi Shirazi, F. Dehghani, *Polymers* **2016**, *8*, 20.
[43] P. A. Gunatillake, R. Adhikari, *Eur. Cells Mater.* **2003**, *5*, 1.
[44] F. von Burkersroda, L. Schedl, A. Göpferich, *Biomaterials* **2002**, *23*, 4221.
[45] H. Zhang, L. Zhou, W. Zhang, *Tissue Eng., Part B* **2014**, *20*, 492.
[46] Y. Ikada, *J. R. Soc., Interface* **2006**, *3*, 589.
[47] A. Gobbi, C. Scotti, G. Karnatzikos, A. Mudhigere, M. Castro, G. M. Peretti, *Knee Surg., Sports Traumatol. Arthrosc.* **2017**, *25*, 2494.
[48] C. Zhang, Y. Cai, X. Lin, *Arthroscopy* **2016**, *32*, 1444.
[49] Y. He, W. Wang, J. Ding, *Chin. Sci. Bull.* **2013**, *58*, 2404.
[50] A. J. Guerra, P. Cano, M. Rabionet, T. Puig, J. Ciurana, *Materials* **2018**, *11*, 1679.
[51] D. Łysik, J. Mystkowska, G. Markiewicz, P. Deptuła, R. Bucki, *Polymers* **2019**, *11*, 1880.
[52] T. Mosmann, *J. Immunol. Methods* **1983**, *65*, 55.
[53] A. van Tonder, A. M. Joubert, A. D. Cromarty, *BMC Res. Notes* **2015**, *8*, 47.
[54] N. J. Marshall, C. J. Goodwin, S. J. Holt, *Growth Regul.* **1995**, *5*, 69.
[55] T. Zhang, Y. Gao, L. Zhu, Q. Zeng, M. Zhou, *Friction* **2020**, *8*, 594.
[56] T. Zhang, S. Zhou, X. Gao, Z. Yang, L. Sun, D. Zhang, *Acta Biomater.* **2017**, *50*, 462.
[57] Z. Lin, J. Luo, Z. Chen, J. Yi, H. Jiang, K. Tu, L. Wang, *Chin. J. Polym. Sci.* **2013**, *31*, 1554.
[58] S. W. Perry, R. M. Burke, E. B. Brown, *Ann. Biomed. Eng.* **2012**, *40*, 277.
[59] B. Pei, W. Wang, Y. Fan, X. Wang, F. Watari, X. Li, *Regener. Biomater.* **2017**, *4*, 257.
[60] C. Humberto Valencia, *J. Int. Med. Res.* **2019**, *47*, 1705.
[61] P. J. VandeVord, H. W. T. Matthew, S. P. DeSilva, L. Mayton, B. Wu, P. H. Wooley, *J. Biomed. Mater. Res.* **2002**, *59*, 585.
[62] K. Xue, Y. Zhu, Y. Zhang, C. Chiang, G. Zhou, K. Liu, *Int. J. Mol. Med.* **2011**, *29*, 146.
[63] C. L. Murphy, B. L. Thoms, R. J. Vaghjiani, J. E. Lafont, *Arthritis Res. Ther.* **2009**, *11*, 213.
[64] A. Tseng, I. Pomerantseva, M. J. Cronce, A. M. Kimura, C. M. Neville, M. A. Randolph, J. P. Vacanti, C. A. Sundback, *Cartilage* **2014**, *5*, 241.
[65] G. M. Salzmann, A.-K. Calek, S. Preiss, *Arthrosc. Tech.* **2017**, *6*, e127.
[66] C. Levinson, E. Cavalli, D. M. Sindi, B. Kessel, M. Zenobi-Wong, S. Preiss, G. Salzmann, P. Neidenbach, *Orthop. J. Sports Med.* **2019**, *7*, 232596711986761.
[67] S. Darwiche, C. Scaletta, W. Raffoul, D. P. Pioletti, L. A. Applegate, *Cell Med.* **2012**, *4*, 23.
[68] C. R. Fitts, *Groundwater Science*, 2nd ed., Academic Press, Boston, MA **2013**, pp. 23–45.